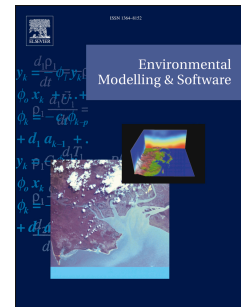


# Accepted Manuscript

Variance based sensitivity analysis of 1D and 2D hydraulic models: An experimental urban flood case

S. Chen, P.-A. Garambois, P. Finaud-Guyot, G. Dellinger, R. Mosé, A. Terfous, A. Ghenaim



PII: S1364-8152(17)31131-3

DOI: [10.1016/j.envsoft.2018.08.008](https://doi.org/10.1016/j.envsoft.2018.08.008)

Reference: ENSO 4273

To appear in: *Environmental Modelling and Software*

Received Date: 24 October 2017

Revised Date: 8 May 2018

Accepted Date: 3 August 2018

Please cite this article as: Chen, S., Garambois, P.-A., Finaud-Guyot, P., Dellinger, G., Mosé, R., Terfous, A., Ghenaim, A., Variance based sensitivity analysis of 1D and 2D hydraulic models: An experimental urban flood case, *Environmental Modelling and Software* (2018), doi: 10.1016/j.envsoft.2018.08.008.

This is a PDF file of an unedited manuscript that has been accepted for publication. As a service to our customers we are providing this early version of the manuscript. The manuscript will undergo copyediting, typesetting, and review of the resulting proof before it is published in its final form. Please note that during the production process errors may be discovered which could affect the content, and all legal disclaimers that apply to the journal pertain.

# Variance based Sensitivity analysis of 1D and 2D hydraulic models: an experimental urban flood case

S. Chen<sup>a</sup>, P.-A. Garambois<sup>a</sup>, P. Finaud-Guyot<sup>b</sup>, G. Dellinger<sup>b</sup>, R. Mosé<sup>b</sup>, A. Terfous<sup>a</sup>, A. Ghenaim<sup>a</sup>

<sup>a</sup>ICUBE-UMR 7357, fluid mechanics team, INSA Strasbourg, 24 Boulevard de la victoire, 67084 Strasbourg cedex, France

<sup>b</sup>ICUBE-UMR 7357, ENGEES, fluid mechanics team, 2 rue Boussingault, 67000 Strasbourg cedex, France

## Abstract

This paper explores spatial sensitivities of 1D and 2D shallow water (SW) models of branched urban flood flows, based on an experimental data-set and a variance decomposition method for various combination of uncertainty sources. General sensitivity patterns of SW model for subcritical flows show that: simulated water height variance is explained upstream by inflow discharge and roughness whereas downstream it is fully explained by downstream water height, influence of lateral inflows propagates in both directions. High sensitivities to roughness can be local in space thus identifying the strongest hydraulic controls for orienting calibration efforts is needed. 2D sensitivities show: the filtering effect of branched network topography on inflow, the zone of influence of boundary conditions, the role of large streets as global flow pattern separators, the difference in roughness sensitivity patterns with 1D. This sensitivity analysis of SW models could be a base for studying flow path and uncertainty propagation.

**Keywords:** Urban Flood, Branched Network, Shallow Water, Sensitivity Analysis, Uncertainty quantification, Variance Decomposition

## 1. Introduction

Flooding is one of the first natural hazard on each continent, and it caused in Europe around 100 billion euros of damage between 1986 and 2006 [28]. In the context of climate change and its possible effects on rainfalls regimes and extremes ([2]), an unprecedented urbanization of floodplains increases the vulnerability of human societies (e.g. [44]). That is why improving the accuracy of flood inundation forecasts and reanalysis combined with uncertainty quantification, especially in urban areas, has become a priority for decision making in civil protection or the insurance industry.

The predictive performances of a model generally depend on model complexity and data availability (e.g. [17] for hydrological models). Flood inundation maps are commonly generated with a 2D Saint-Venant shallow water (SW) model consisting in depth averaged Navier-Stokes equations (e.g. [4, 24, 30]) where uncertainty sources can stem from the model structure or the parameterization (e.g. basal friction), or the initial and boundary conditions (bathymetry and source terms). A full shallow water model including inertia terms may be required to capture small scale features and rapidly varying flows over “rural” floodplains (e.g. [31]), along with appropriate numerical methods for shock capture and wet dry front treatments (e.g. [30]). As a matter of facts, the interaction of high energy flows with obstacles triggers 3D flow processes such as crossroads junctions ([27]) - which for a realistic representation generally require to solve the Navier-Stokes equations in 3D. Consequently, flow resistance parameterization for a 2D SW model, which is an effective representation of 3D (turbulent) free surface flow structures, may depend on its scale for localized head losses in complex geometries (e.g. [18]) or parietal friction on smooth or macro roughness (e.g. [7, 8]). Another boundary condition known to be a source of uncertainty is inflow discharge especially in complex urban flood configurations - which can be provided by in situ measurements (involving rating curve uncertainty [10, 32, 41]) or simulated by a hydro-meteorological chain involving meteorological model uncertainties [43] and hydrological model uncertainties (e.g. [12]).

Given the importance of uncertainty estimation in flood modelling and forecasting, this contribution presents a thorough sensitivity analysis (SA) of 1D Saint Venant and 2D SW models to

their (uncertain) parameters and boundary conditions. The study focuses on the case of urban flood flows in a complex streets network, based on a fine and unprecedented laboratory scale experiment while in situ flood data are still rare ([14]). Remark this streets network is composed of several 4 branch crossroads creating complex patterns of free surface flows confluences and diffluences.

Flood simulation accuracy is not necessarily improved by increasing model complexity and resolution (cf. [11]) but uncertainty sources may also vary (even interact) as the amount of data required to constrain the model. Sensitivity analysis has become a popular tool in environmental modelling (e.g. [33]) for assessing how the uncertainty in the output of a model can be apportioned to different sources of uncertainty in the model input ([39]). SA is used in catchment hydrology to explore high dimensional parameter spaces, assess parameter identifiability and understand uncertainty sources ([5, 15, 16, 25, 34] among others). Temporal variations of distributed rainfall-runoff and simplified hydraulic model parameters sensitivities are analyzed and ranked in the case of Mediterranean flash floods ([15]) or large scale conceptual model of the Amazon river ([13]). Temporal sensitivities of simulated flood response highlight the importance of phases and locations to runoff production parameters and/or runoff routing depending on rainfall forcing and soil properties variabilities but also drainage network shape among other parameters.

Among the few SA studies in the field of river hydraulic modelling, [36] propose a generalized sensitivity analysis of a 1D SW model with simplified geometry adapted to remote sensing and ungauged rivers, in the case of flood scenario on the Lèze River, France. The authors show the importance of downstream flow depth in controlling flood extent for a 1.5 km reach of a small river (around 100m bankfull width). [20] propose local sensitivity equations for the 2D steady state SW equations without shocks and provide some guidelines for model calibration and validation. These sensitivity equations are also derived and implemented for 1D SW model ([9]). Local sensitivities derived with the adjoint method, and involving a cost function, are presented in the case of a high resolution model (2D SW DassFlow software) of a flood on a 2km reach of the Lèze River [30]. The authors find higher sensitivities of water depth to bathymetry and roughness downstream (subcritical regime) of the observation points in the floodplain and in the main channel, roughness sensitivity is higher in the main channel. Recently variance based on SA has been applied to 2D hydraulic models in flooding conditions ([1, 41]). [1] present a spatial SA approach of a 2D SW model based on high resolution digital elevation model (DEM). Sensitivity maps of simulated water depth to uncertain parameters including topography are presented for the last 5km of the Var valley, France - November 1994 flood. For a 50km<sup>2</sup> rural floodplain in Sicily, [41] highlight the sensitivity of simulated flood extent to inflow discharge during flood rising limb then the channel friction parameter during flood peak and the floodplain friction parameter during recession. First order sensitivity of both maximal water depth and flood extent to topography and model resolution is limited whereas interactions of those parameters with others (hydrographs and roughness) increases at the end of the flood given their influence on floodplain flowpathways in this case. These few recent SA studies mostly bring insight in first order hydraulic model sensitivity of its parameters for common subcritical flood flow cases in simple channels on the order of few km and rural floodplains.

This paper investigates first order sensitivities of 1D and 2D hydraulic model outputs (water height and discharge) to their parameters and possible interactions, in the case of floods flows through a whole district, involving complex 3D flow structures from the street scale to the district scale. A thorough quantitative sensitivity analysis of the widely used 1D and 2D Saint Venant SW models with a variance based method is proposed ([35, 38]). A unique experimental dataset at the horizontal scale  $1/200$  is used, with urban flood flows corresponding to frequent to rare return periods ([14]). Therefore the originality of this paper is to explore the sensitivities of 1D and 2D SW models of branched urban flood flows, involving many subcritical confluences and diffluences but also few supercritical flow zones based on a detailed experimental data-set. The detailed sensitivity maps assessing the relative importance of input parameters and depicting the main hydraulic controls provide valuable guidance for the calibration of hydraulic models and for the design of experimental models.

The sensitivity of 1D and 2D SW model outputs (water height for 1D and water height and discharge for 2D) to their parameters is investigated including: global and local boundary conditions (water heights and discharge) and spatially uniform or distributed friction coefficient respectively tested in various ranges centered around their calibrated values. For various experi-

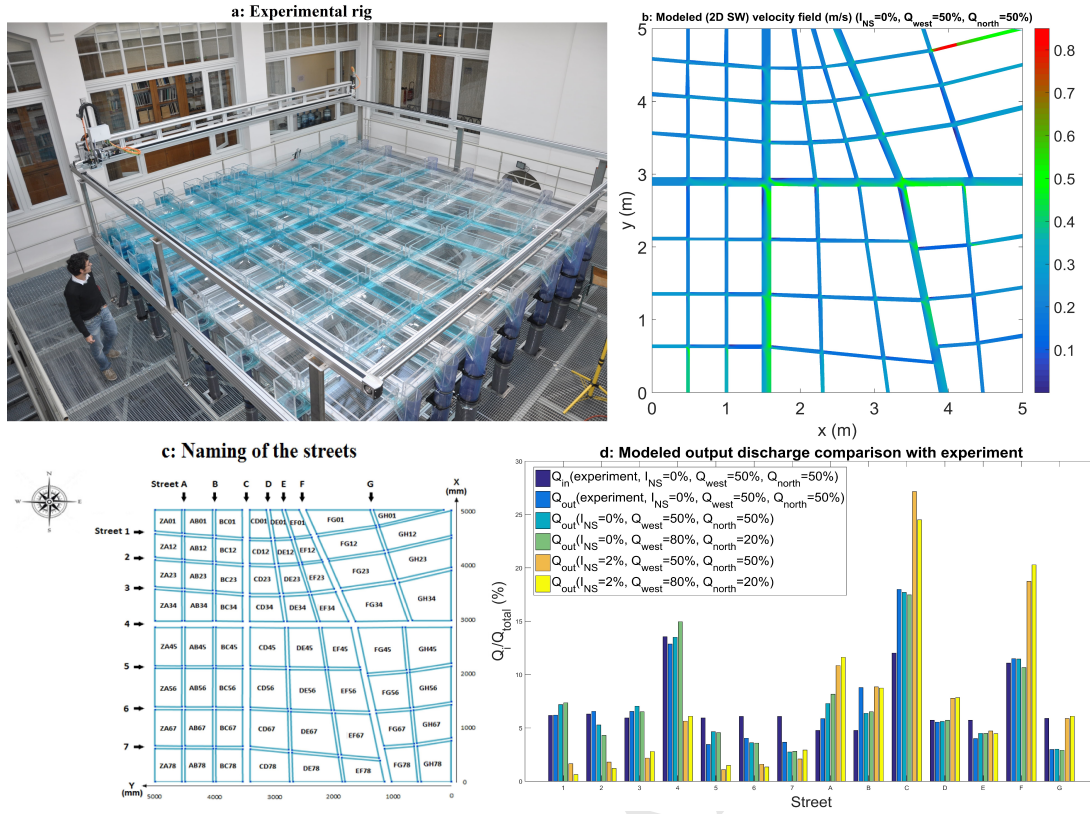


Figure 1: (a) Experimental rig, (b) modeled (2D SW) velocity field for  $Q = 80m^3/h$  equidistributed between upstream west and north faces, (c) naming of the streets and (d) modeled output discharge (2D SW model with roughness  $K_{2D} = 100m^{1/3}.s^{-1}$ ) compared with experiment.

mental configurations a variance decomposition method (ANOVA) is used to calculate spatially distributed Sobol sensitivity indices (Si's). The sensitivities of input parameters are analyzed on two main streets and the whole urban district using respectively 1D and 2D models.

The paper is organized as follows. Section 2 describes the GSA method and the computation of Sobol indices, experimental device and numerical models used to investigate urban flood flows controls. Spatial patterns of the sensitivity of simulated water height to parameters are presented in section 3 both for 1D and 2D models. 10 parameters of the 1D model are investigated first then the three most sensitive parameters, or lateral inflows or distributed roughness are studied separately. 2D sensitivity maps are then presented. Section 4 presents a detailed discussion around sensitivity patterns in various configurations including: a discussion about 1D/2D roughness meaning, the estimation of Sobol indices on a hydraulic jump, the sensitivity of modeled (2D) outlet discharges and the effect of bathymetric slope. Conclusions and perspectives are presented in section 5.

## 2. Methods and models

### 2.1. Experimental rig and numerical models

This study is based on the urban flood experimental rig designed and built at the ICube laboratory in Strasbourg (France) [3, 14]. It is supposed to be representative for typical urban geometries at the horizontal scale  $1/200$  with street widths of  $12.5cm$  and  $5cm$  as well as various crossroad angles. It is composed of 64 impermeable blocks on a  $5m \times 5m$  horizontal plan. The streets network is composed of seven streets in the north-south direction crossed by seven streets in the west-east direction (see figure 1 - c). The inflow discharge of each street of the north and west faces is supplied by a volumetric pump, a rectangular weir controls water levels at the outlet of each street and outlet discharges are measured using calibrated weirs relationships [14]. The studied configurations correspond to steady state experiments and the corresponding boundary conditions are presented in Appendix (table 2).



1D and 2D steady models are used for flow simulations under experimental conditions. 1D **modelling** is performed for widest streets C and 4 using 1D **SW** equations which are solved with a finite volume approach (e.g. [6, 19]) using a classical HLLC Riemann solver [22]. 2D **modelling** is performed for the whole experimental rig using Telemac2D [23] which solves the 2D shallow water equations **coupled to a classical  $k-\varepsilon$  closure turbulence model** using a finite volume approach on unstructured triangular mesh.

2D model is run with upstream discharge and downstream water **height** determined from experimental data. Roughness is calibrated with a trial and error procedure in order to **better** match outlet discharges and measured flow lines (cf. figure 1 - d and section 3.2.1). 1D model is run with experimental data for the lateral discharge and downstream water **height**, and its roughness is calibrated analogously in order to best match measured flow lines (cf. figure 4 - top and section 3.1.1). **The sensitivity of 1D flow lines and 2D distributed water height and outlet discharges are investigated in the following.**

## 2.2. Background on model analysis with variance decomposition methods

Let us distinguish two methods assessing the uncertainty associated with the model outputs and their sensitivity to input parameters:

- **Uncertainty quantification (UQ)** is the forward propagation of uncertainty to predict the overall uncertainty in model outputs.
- **Sensitivity analysis (SA)** is the study of how the uncertainty in model output can be apportioned to different sources of input uncertainties ([38, 33]). It includes local sensitivity analysis that evaluates the effect of a small perturbation of the considered input parameters around a specific value to model outputs ([9, 20, 21, 30]); and global sensitivity analysis that explores model behavior over a whole parameter space but that is often more computationally expensive (e.g. [33]).

Both methods are based on a sampling of model input parameter space. The result of multiple model evaluations on this sample of parameter sets can be represented in terms of probability distributions of the output values (UQ) or relative weights of the input parameters in explaining the variability of model output (SA). A variance decomposition method is used for performing sensitivity analysis of SW models in this paper.

For a generic model  $f$ , let  $\Omega^k \in \mathbb{R}^k$  denote the set of all possible values that the model parameters can take. Let  $\underline{X} \in \Omega_k$  be a possible value of the  $k$  model parameters normalized by their variation range. We denote by  $Y = f(\underline{X}) = f(X_1, X_2, \dots, X_k)$  the relationship that links the model inputs to the model output. **Following [40, 37] and using a high-dimension model representation with functions orthogonal in pairs (in the sense of the scalar product  $\int_{\Omega_k}$  - leading to variances) the so-called functional ANOVA decomposition can be obtained:**

$$V(Y) = \sum_i V_i + \sum_i \sum_{j>i} V_{ij} + \dots + V_{1,2,\dots,k} \quad (1)$$

where  $V(Y)$  is the total variance,  $V_i = \text{Var}_{X_i}(E_{X \sim i}(Y|X_i))$  is the first-order variance caused by parameter  $X_i$ ,  $V_{ij} = \text{Var}_{X_{ij}}(E_{X \sim ij}(Y|X_i, X_j)) - V_i - V_j$  is the covariance caused by  $X_i$  and  $X_j$  (second-order variance), and higher order terms show the variance contribution from multiple parameters.

The sensitivity index of first-order effect of  $X_i$  on  $Y$  can be defined as:

$$S_i = \frac{V_i}{V} \quad (2)$$

where  $S_i$  is the Sobol index, always between 0 and 1. The sum of all Sobol indices is equal to 1:

$$\sum_{i=1}^k S_i + \sum_{i<j}^k S_{ij} + \dots + S_{1,2,\dots,k} = 1 \quad (3)$$

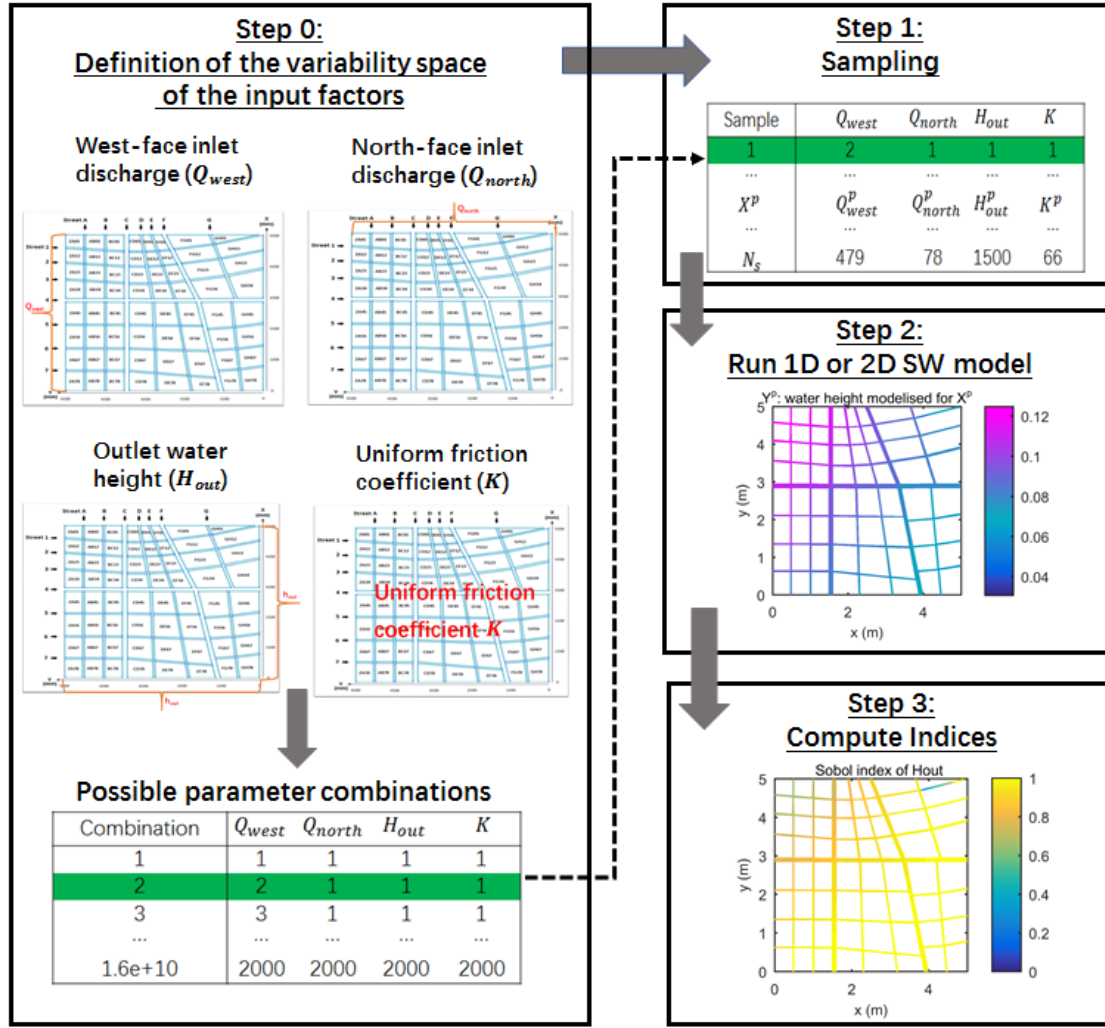


Figure 2: Main steps of the methodology used for performing the Global Sensitivity Analysis (GSA) of 1D or 2D hydraulic models. Step 0 consists in choosing the parameters to test and defining their physical bounds hence defining parameter space. Each parameter is sampled randomly in step 1. Next, hydrodynamic model is run for each parameter set in step 2 and sensitivity indices are calculated for all those model realizations in step 3.

### 2.3. Sobol indices computation method

Variance based (Sobol) sensitivity indices are calculated in this paper for 1D and 2D SW models following the general method exposed in figure 2. It is based on a large sample of size  $N_s$  of parameters vectors  $\underline{X}^p = (X_1^p, X_2^p, \dots, X_k^p)$ ,  $p \in [1..N_s]$ , considered in this study as a stochastic variables. Sobol indices are computed from the sample of hydraulic model outputs  $Y^p$  using a state dependent parameter metamodeling as proposed by [35]. The metamodeling approach is based on a State Dependent Parameter (SDP) modelling, which is a model estimation approach based on recursive filtering and smoothing estimation. It is a simple and computationally effective method, based on a sample of parameter space, for approximating the model under analysis and estimating conditional variances of model output with respect to each parameter. The bounds of the variability space of input parameters  $\underline{X}^p$  are defined around their calibrated values. The different tested combinations of hydraulic parameters and boundary conditions along with parameter ranges are explained for each numerical experiment in what follows.

## 3. Results

This section details sensitivity analysis of 1D and 2D SW models. The sensitivities to their parameters are investigated with the GSA method exposed above (cf. 2.1) for 1D hydraulic models of the two main streets of the experimental rig and for full 2D models (cf. figure 1). The spatially distributed variances of model outputs are decomposed with respect to different

hydraulic parameters. Each input parameter vector  $\underline{X}^p = (X_1^p, X_2^p, \dots, X_k^p)$ ,  $p \in [1..N_s]$  is formed by:

- Inflow discharges including lateral inflows for 1D model
- Downstream water [heights](#)
- Roughness (uniform or spatially distributed)

Different combinations of uncertainty sources, i.e. parameter combinations, and uncertainty ranges are investigated for the 1D model first (section 3.1). For the 2D model, [parameters](#) ranges are chosen corresponding to uncertainty ranges [of](#) our experimental dataset (cf. [14]) (section 3.2).

### 3.1. Sensitivity analysis [of water height](#) in 1D configuration

#### 3.1.1. Model Calibration

Before conducting the GSA, a calibration of the 1D model is needed, it is performed with uniform or distributed roughness coefficient. The calibration aims at minimizing the Euclidean norm between simulated and measured flow lines. Given the small number of parameters a trial and error procedure is used. The calibrated roughness and 1D model inputs with their variation ranges are presented in table 1. For uniform roughness, the Strickler coefficient found for street C is  $K_C^{cal} = 21.5m^{1/3}.s^{-1}$  and for street 4  $K_4^{cal} = 21m^{1/3}.s^{-1}$ . The calibration results for distributed roughness consist in a roughness value for streets:  $K_{Cs}^{cal} = 26.5m^{1/3}.s^{-1}$  for street C and  $K_{4s}^{cal} = 28.5m^{1/3}.s^{-1}$  for street 4 and in a value for crossroads:  $K_{Cc}^{cal} = 9.5m^{1/3}.s^{-1}$  for street C and  $K_{4c}^{cal} = 9m^{1/3}.s^{-1}$  for street 4. Figure 4 illustrates the simulated water height profiles with uniform and distributed roughness compared with experimental values. Distributed roughness slightly improves simulated water [height](#) profile. Recall that flows are characterized by complex 3D hydrodynamic structures, but this contribution focuses on comparing the sensitivities computed for 1D and 2D [modelling](#) approaches in a branched hydraulic network.

#### 3.1.2. Sensitivity of GSA on 10 parameters to sampling range

Sensitivity of Sobol indices estimation to parameter sampling range has been tested by applying the same ranges to all tested parameters from 5% to 60%. A limited influence on sensitivity indices values is observed and sensitivity patterns are relatively unchanged (i.e. proportion of the output variable variance explained by each parameter) (cf. figure 3). The influence of unequal ranges has also been tested and is presented in following sections for ranges corresponding to experimental uncertainties. The sensitivity to sample size has been investigated  $N_s \in [100; 10000]$ , and the choice is made to use a sufficient number of 2500 parameter sets ensuring good convergence of  $S_i$ s estimation for each following experiment.

Interestingly, figure 3 shows the spatial variation of first order sensitivities of 10 parameters. The sum is close to one along the streets highlighting very few interaction effects between the 10 tested parameters in explaining modeled water [height](#) variance. It is mainly explained by three parameters over the (equal) tested ranges: roughness, upstream discharge and downstream water [height](#). Those three parameters explain about one third of [the water height](#) variance upstream of street C. The influence of both upstream discharge and roughness [decreases](#) along flow distance whereas the influence of downstream water [height](#) increases [steadily](#) to reach more than 95% downstream. This is a reasonable pattern for a subcritical flow.

#### 3.1.3. GSA on ten parameters with experimental uncertainties

This section investigates the sensitivity of 1D simulated flow lines to boundary conditions and source terms. Sensitivities are presented for the main streets C and 4 of the urban flood rig, conveying around 30% of the total flow (cf. figure 1). Ten input parameters are considered including upstream inlet discharge  $Q_{in}$ , outlet water height  $h_{out}$ , uniform roughness  $K$  and seven lateral discharges corresponding to mass exchange at crossroads  $Q_{\{1, \dots, 7; A, \dots, G\}}$  (cf. table 1). The variation range of each input parameter around its calibrated value ( $^{cal}$ ) is chosen corresponding to the experimental uncertainties. The ranges considered here are:  $Q_{in}^{cal} \pm 5\%$ ,  $h_{out}^{cal} \pm 10\%$ ,  $K^{cal} \pm 50\%$  and  $Q_{\{1, \dots, 7; A, \dots, G\}}^{cal} \pm 5\%$ ; note that each lateral discharge is perturbed independently.

The spatial variations of Sobol indices of [the](#) ten input parameters are presented in figure 4 with parametric uncertainty ranges corresponding to experimental ones. In that case, the sum

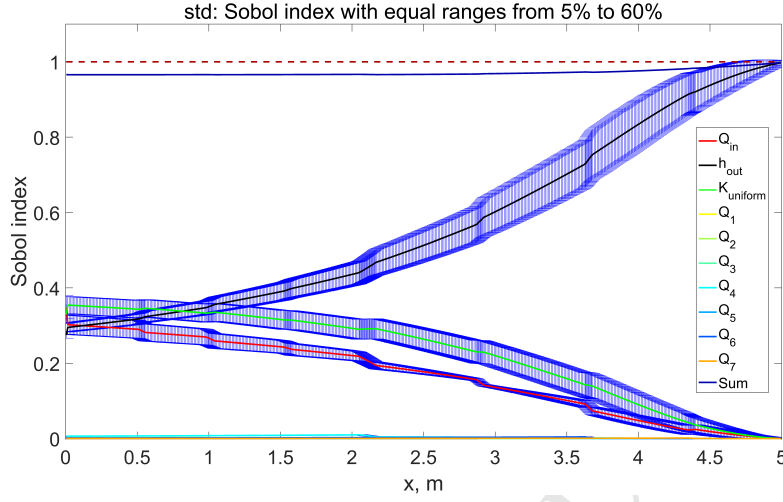


Figure 3: Sobol index estimated for parameters sampled on equal ranges of amplitudes [varying from  \$\pm 5\%\$  to  \$\pm 60\%\$](#) .

Table 1: Parameters used and associated perturbation ranges for the 1D street [modelling](#)

Symbol	Meaning	Value (street C)	Value (street 4)	Range
$Q_{in}$	Street C (4) inflow discharge	$2.67l/s$	$3.01l/s$	$\pm 5\%$
$h_{out}$	Street C (4) outflow water height	$0.083m$	$0.078m$	$\pm 10\%$
$Q_1(Q_A)$	Lateral street 1 (A) inflow discharge	$0.171l/s$	$0.014l/s$	$\pm 5\%$
$Q_2(Q_B)$	Lateral street 2 (B) inflow discharge	$0.198l/s$	$0.155l/s$	$\pm 5\%$
$Q_3(Q_C)$	Lateral street 3 (C) inflow discharge	$0.093l/s$	$-0.107l/s$	$\pm 5\%$
$Q_4(Q_D)$	Lateral street 4 (D) inflow discharge	$0.407l/s$	$0.261l/s$	$\pm 5\%$
$Q_5(Q_E)$	Lateral street 5 (E) inflow discharge	$0.237l/s$	$0.077l/s$	$\pm 5\%$
$Q_6(Q_F)$	Lateral street 6 (F) inflow discharge	$0.296l/s$	$0.380l/s$	$\pm 5\%$
$Q_7(Q_G)$	Lateral street 7 (G) inflow discharge	$-0.319l/s$	$-0.553l/s$	$\pm 5\%$
$K$	uniform roughness coefficient	$21.5m^{1/3}.s^{-1}$	$21m^{1/3}.s^{-1}$	$\pm 50\%$
$L$	Domain length	$5m \times 0.125m$	$5m \times 0.125m$	
$\Delta x$	Cell size	$0.02m$	$0.02m$	

of first order indices  $S_{i \in [1..10]}$  is very close to one indicating very few higher order interactions among parameters. The results for both street C and 4 show that the main flow controls over the tested uncertainty ranges are the roughness, downstream water height and upstream discharge. The remaining sensitivities of the seven lateral discharges are very small compared to the three other parameters. Therefore, for the sampled ranges, those ten input parameters are studied separately in subsequent sections: three main parameters and seven lateral discharges.

#### 3.1.4. GSA on the three main parameters

The spatial variation of Sobol indices of the three main parameters (upstream discharge, downstream water height and friction) sampled in experimental uncertainty ranges are presented in figure 4. Results for both street C and 4 show that the sum of all three parameters is close to 1 highlighting negligible interactions effects among those three parameters. The modeled water height variance is mainly explained by the roughness and the downstream water height for the whole streets length. Upstream of street C or 4, roughness explains more than 95% of model response and its influence steadily decreases with increasing flow distance towards to downstream. The opposite pattern is obtained for downstream water height sensitivity with  $S_{h_{out}}$  greater than 95% downstream. Flow in both streets C and 4 is subcritical everywhere and such a pattern corresponding to downstream hydraulic control is logical. There are no interaction effects between those three parameters along street C and 4, and water height variance is perfectly explained by their first-order Sobol indices. In magnitude, the influence of the inlet discharge can be neglected for the tested ranges compared to those of water height and friction coefficient.

#### 3.1.5. GSA on lateral discharges

We consider here the case where uncertainty sources are only the lateral discharges. The spatial patterns of Sobol indices are presented in figure 5. Their sum stays close to one along street C or 4 and again shows negligible interaction effects. The sensitivity of output water height to a given lateral discharge is maximal at its inflow point (crossroad). Interestingly the influence of a lateral mass flux propagates to the downstream outlet but also upstream in subcritical flow conditions as a downstream control. After the last crossroad, the Sobol indices of lateral discharges stay constant and their values are proportional to lateral discharge values which can be correlated to the imposed water height at the downstream end of the street:  $S_{Q_i} = \alpha Q_i^2 \forall i \in [1, 2, 3, 4, 5, 6, 7; A, B, C, D, E, F, G]$  where  $S_{Q_i}$  stands for the Sobol index at the downstream end to the lateral discharge of street  $i$  and  $\alpha$  is a constant factor.

#### 3.1.6. GSA on distributed roughness

The spatial pattern of water height sensitivity to a uniform roughness has been studied in section 3.1.3 and 3.1.4. Now the influence of a distributed roughness pattern for streets ( $K_s$ ) and crossroads ( $K_c$ ) is considered. The variation ranges of two roughness are both set to 50% around their calibrated values (cf. section 3.1.1); the ranges for the other parameters are the same. The results show that no interaction effect exists between those two input parameters since the sum of first order  $S'_i$ s is close to 1 in each street (figure 6). For both streets,  $K_s$  has an increasing influence on water height variance with increasing flow distance contrarily to crossroad roughness sensitivity that decreases.

Interestingly, the sensitivity profile between two crossroads (identified by the vertical dashed lines) evolve from linear upstream to parabolic downstream. This might be explained because the friction term (involving the roughness  $K$ ) is proportional to  $v^2$  and as the water height decreases along the street, the velocity increases. Remark also that the magnitude of the sensitivity jump at the crossroads is correlated to the magnitude of the lateral injection.

Interestingly, crossroads roughness plays a more important role (up to 55%) for street 4 than for street C (only up to 34%). This demonstrates that a best effort modelling of the “same” domain (street C or street 4) would not be achieved using the same parameter ( $K_c$  for street 4 and  $K_s$  for street C). This highlights that the importance of the roughness parameter is not related to the area of the modeled domain on which the parameter applies, the crossroads representing 15% of it.

### 3.2. Sensitivity analysis in 2D configuration

#### 3.2.1. 2D SW model set up and calibration

2D steady state SW simulations are performed for the whole experimental rig in order to better reproduce complex flow structures (cf. [4, 42]). The boundary conditions are based on



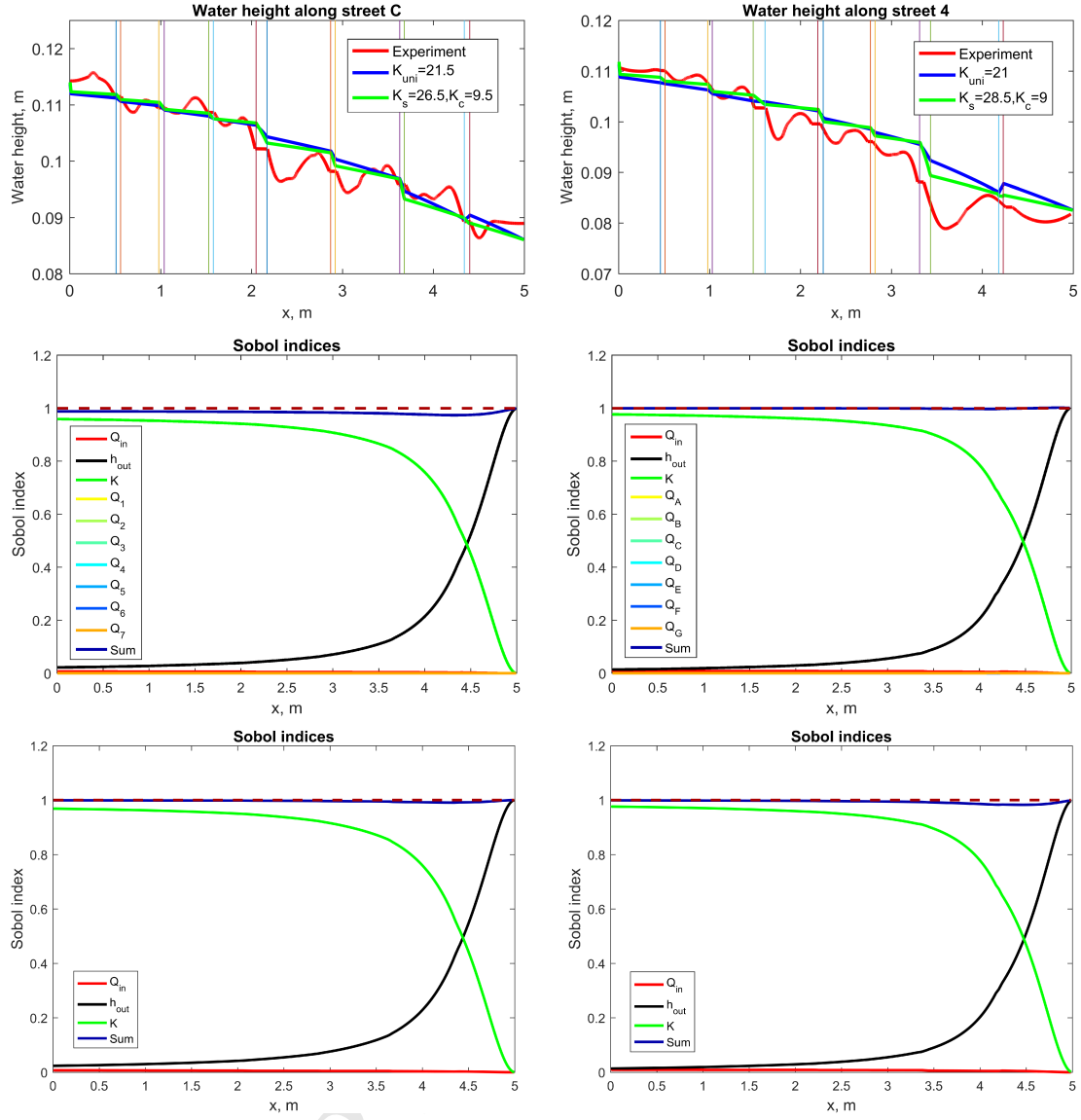


Figure 4: Top: Comparison of the computed and measured water height profiles and Sobol indices of ten (Middle) and three (Bottom) main input parameters. The results are plotted for streets C (Left) and 4 (Right). For Sobol index of 10 parameters,  $S_{Q_i} < 0.002$ ,  $\forall i \in [1, 2, 3, 4, 5, 6, 7; A, B, C, D, E, F, G]$ , over experimental uncertainty ranges (cf. table 1)

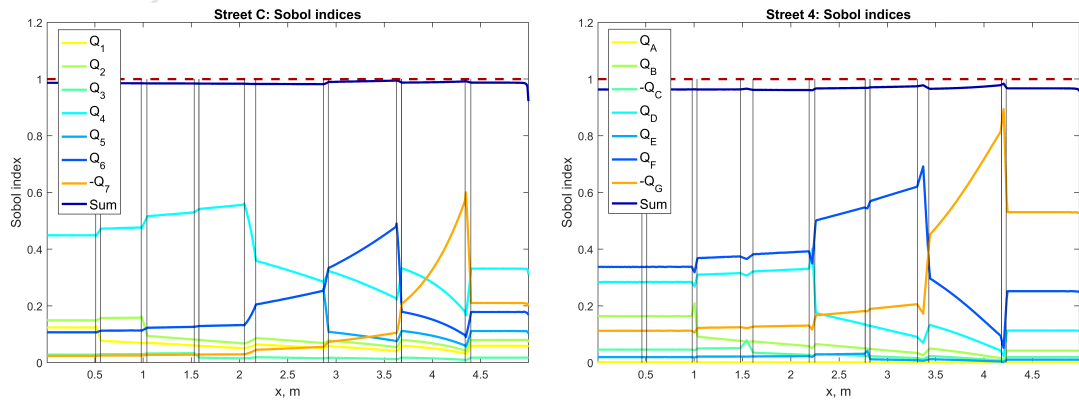


Figure 5: Sobol indices of seven lateral discharges with minus signs for flow loss.

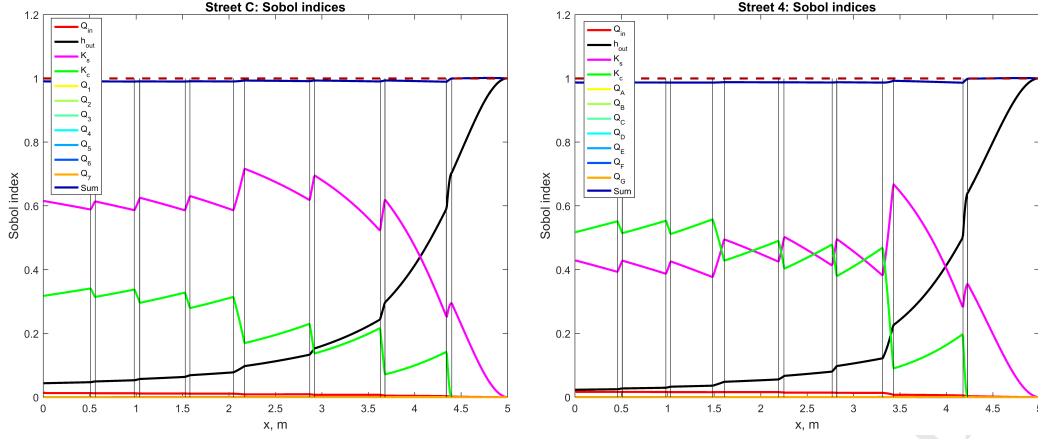


Figure 6: Sobol indices of distributed roughness (For street C,  $K_s = 26.5m^{1/3}.s^{-1}$  and  $K_c = 9.5m^{1/3}.s^{-1}$ ; For street 4,  $K_s = 28.5m^{1/3}.s^{-1}$  and  $K_c = 9m^{1/3}.s^{-1}$ .)

the experimental data-set listed in Appendix table 2. Constant discharges and water heights are prescribed at inlets and outlets along with a spatially uniform friction coefficient ( $K_{2D} = 100m^{1/3}.s^{-1}$ ), since it is only calibrated with measured outlet discharge distribution (see figure 1 d). Remark that contrarily to 1D model calibrated on measured water height profiles given known discharge, the 2D model is only calibrated against outlet discharges to reproduce the correct flow pattern within the urban district.

Note that a mesh convergence analysis has been performed for cell sizes ranging between 0.01 and 0.0025m, a 0.005m cell size is finally selected. A total inflow discharge of  $80m^3.h^{-1}$ , corresponding to rare and high flood flow, is used for steady state simulations with different inflow discharge partitions between west and north face: 1) 50% west and 50% north; 2) 80% west and 20% north. Within a face, the discharge is divided proportionally to the street width. The spatial distributions of simulated water height and Froude number are presented in figure 7 for the two inflow repartitions. Water height decreases from west-north corner to south-east corner in both configurations. The flow over the whole district is subcritical except in street 1 after the last crossroad between street 1 and G, where a supercritical flow zone occurs. The unequal flow repartition with increased inflow at 80% on west face increases the water height at south-west corner and reduces the region of supercritical flow in street 1 close to the outlet. Interestingly, the outlet street discharges modeled in both configuration (50-50% and 80-20%) are very similar and correspond to the experimental measurements (figure 1). These results highlight the filtering effect of the urban geometry on the inflow discharge as demonstrated in [14].

### 3.2.2. GSA on water height

Based on previous investigations with 1D model (cf. section 3.1.3), four main input parameters are tested using GSA, namely west-face discharge  $Q_{west}$ , north-face discharge  $Q_{north}$ , outlet water height  $h_{out}$  and uniform friction coefficient  $K$ . Again their variation ranges are determined based on experimental uncertainties ( $Q_{north}^{cal} \pm 5\%$ ,  $Q_{west}^{cal} \pm 5\%$ ;  $h_{out}^{cal} \pm 10\%$  and  $K^{cal} \pm 50\%$ ). A sample size  $N_s = 2000$  ensures a good convergence of Sobol indices estimation in this 2D SW model configuration (cf. section 3.1.1). Sensitivity pattern of water height is presented through 2D maps of Sobol indices along with their sum for the two inflow discharge partitions (figure 7). The sum of all Sobol indices is close to 1 for subcritical flow zones (corresponding to Froude number below 1 in figure 7) meaning water height variance is perfectly explained by the first-order Sobol indices of the tested parameters. Interestingly, the sum  $\sum S_i$  is significantly below 1 in the part of street 1 in which a supercritical flow zone and a hydraulic jump appear for some parameter sets. A detailed investigation of this particular point is made in section 4.2.

2D maps of first order sensitivities of the water height to the four tested parameters are presented in figure 7b, c, d, e. For the 50-50% hydraulic configuration, the roughness and the downstream water height are the most important parameters explaining the output water height variance; as found for the 1D model (cf. section 3.1.3). Water height sensitivity to downstream water height  $h_{out}$  and roughness  $K$  evolves globally in the direction from the north-west corner

to the south-east corner except in the circle corresponding to supercritical flows; both patterns evolve as for the 1D GSA: decrease (resp. increase) in the direction of the flow for the sensitivity to  $K$  (resp.  $h_{out}$ ). The sensitivity to upstream discharge decreases along effective flow direction, i.e. along the diagonal from north-west to south-east corner; and is almost null in the downstream part of the streets. Interestingly, for the 50-50% configuration the maps show:

- the maximal sensitivity to both upstream discharge (that has the same nominal value and the same range of variation) is almost **twice larger** for  $Q_{west}$  than for  $Q_{north}$ ;
- the water **height** is more sensitive to upstream discharge in 2D than in 1D. This might be explained by the fact that discharge is more free on the 2D domain than on the 1D. As the **modelling** is performed in steady state, the water surface profile between two crossroads is described by a classical backwater curve that is function of the discharge (between other parameters). Indeed in 1D, the discharge is totally imposed by the upstream value and the lateral inputs on one street whereas in 2D, the flow repartition between street remains free (driven by the **modelled** crossroad behavior and mass exchanges between streets).

Histograms presented on figure 8 show the sensitivity of water **height** to the tested parameters for several precise locations consisting mainly in crossroads within the streets network. They are ordered by increasing hydraulic distance from the upstream north-west corner. It depicts clearly the decrease of water **height** sensitivity to upstream controls:  $Q_{west}$ ,  $Q_{north}$ ,  $K$ .

Figure 7 shows sensitivity patterns for a 80-20% inflow discharge partition between west and north faces. Spatial Sobol index patterns for this asymmetrical inflow are similar to the ones for the 50-50% configuration. However, the patterns are oriented from the north-west to the south-east corner; i.e. oriented in the direction of the global flow. As **expected**, the Sobol index of north-face discharge decreases, whereas west-face discharge index increases and explains more than 25% of water **height** variance for streets 1 to 4. In that case, the influence of downstream control ( $h_{out}$ ) is lower for the region close to the west and north faces. The supercritical flow region downstream of street 1 is also reduced for less discharge passing by from the north-face.

## 4. Discussion

### 4.1. Head losses modelling

*Concerning classical shallow water models (cf. Appendix equations (4) and (5)), a unique source term  $S_f$  is generally used to model all head losses, i.e. flow energy dissipation. The empirical Manning-Strickler friction law is generally used with a unique (or spatially distributed) Strickler friction coefficient calibrated such as a SW model reproduces flow depth and discharge at some reference points/sections. In such case this coefficient is intended to account for the basal and wall friction plus other dissipative effects including turbulence.*

*Note that in the case of a 1D model, the red curve on figure 4 (top), corresponding to the experimental flow lines averaged in width, show a convexity in water height profiles along this street downstream each crossroad where a recirculation area appears (cf. [29]). In such case the effective flow vein is narrowed and the flow accelerates; with a contraction coefficient  $0 < \alpha < 1$  the effective cross sectional area  $A_{flowvein} = \alpha A_{fullwidth}$ . This significant increase of the velocity makes the friction larger ( $S_f \propto U^2$ , with  $U = Q/A$ ). The 1D model presented in this study is based on the full street width and thus needs an effective friction parameter value to reproduce the flow reference (i.e. a higher friction on the full width). In other words, the model roughness coefficient  $K_{1D}$  is calibrated such as the friction slope of the 1D model  $S_{f1D}$  best reproduces the experimental one  $S_{fexpe}$  at “large scale” between two crossroads:  $S_{f1D} = \frac{Q^2}{(A)^2 K_{1D}^2 R_{h1D}^{4/3}} =$*

*$S_{fexpe} = \frac{Q^2}{(\alpha A)^2 K_{expe}^2 R_{hexpe}^{4/3}}$ , hence  $K_{1D} = (\alpha + \epsilon(\alpha)) K_{expe}$  with  $\epsilon(\alpha)$  a small error on  $\alpha$  due to the difference on hydraulic radius estimation in the tested width-depth ranges. This explains the lower value found for  $K_{1D} \sim 21.5 m^{1/3} \cdot s^{-1}$  after calibration in this paper compared to an expected value of  $80 - 100 m^{1/3} \cdot s^{-1}$  for plexiglass walls.*

2D SW models are able to model recirculation zones and mixing layers (recall with depth averaged velocities) and then the corresponding localized head losses, hence it is not necessary to account for those effects with the friction coefficient. The uniform roughness calibrated in this study for the 2D SW model (**including a  $k - \epsilon$  turbulence model as suggested by [4] for better simulating recirculation zones**) is  $K_{2D} = 100 m^{1/3} \cdot s^{-1}$ . This latest value is a good

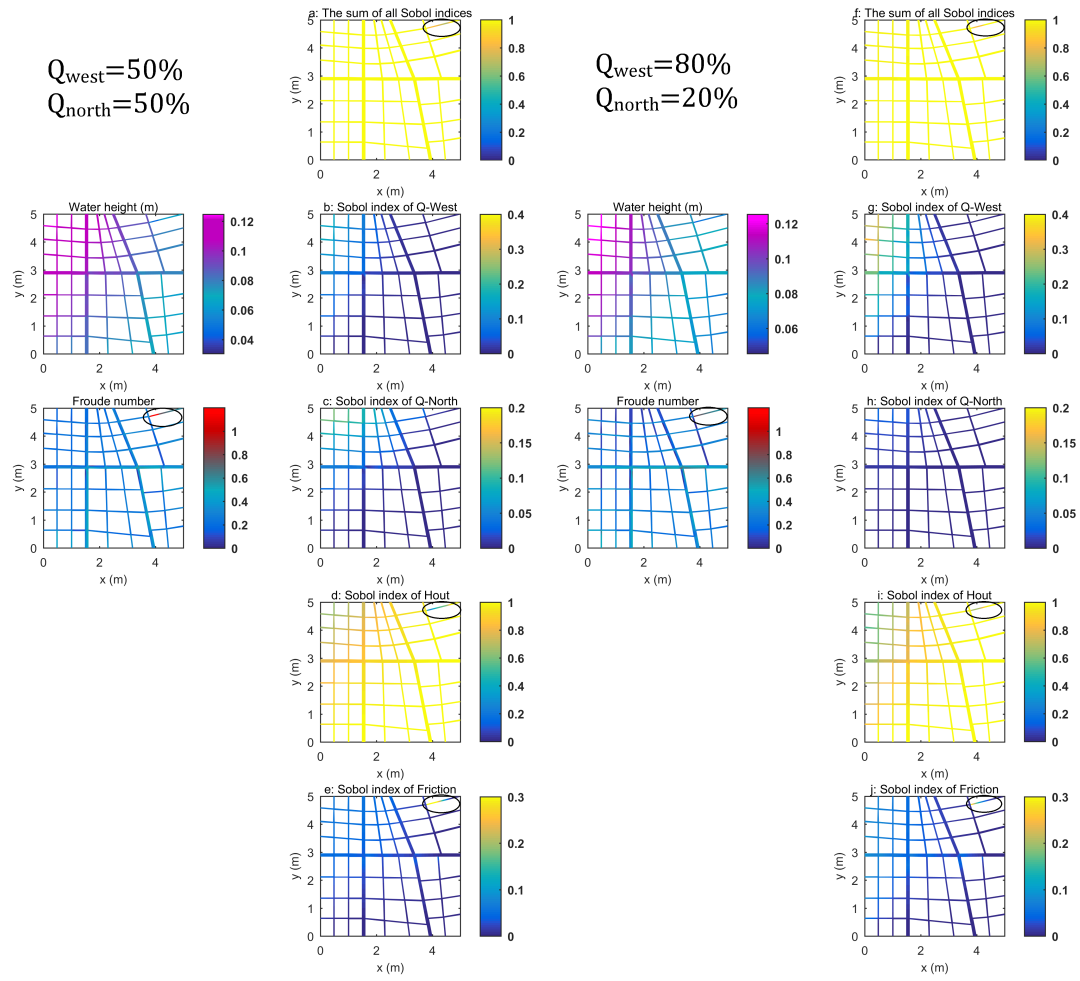


Figure 7: 2D maps of Sobol indices for  $80 \text{ m}^3/\text{h}$ : Left, inflow discharge partition at west and north-face 50-50%; Right, inflow discharge partition at west and north-face 80-20%. The circles highlight supercritical flow zones ( $Fr > 1$ ).

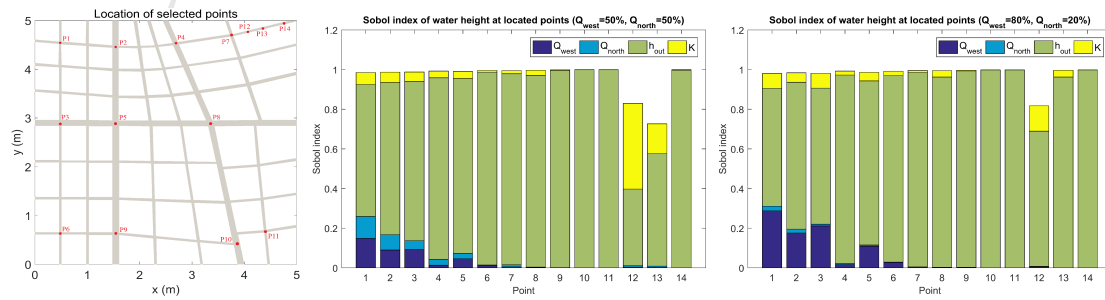


Figure 8: Decomposition of local sensitivity of water height to the tested parameters, experiment without slope. Numbering of points made in function of hydraulic distance to the upstream north-west corner.

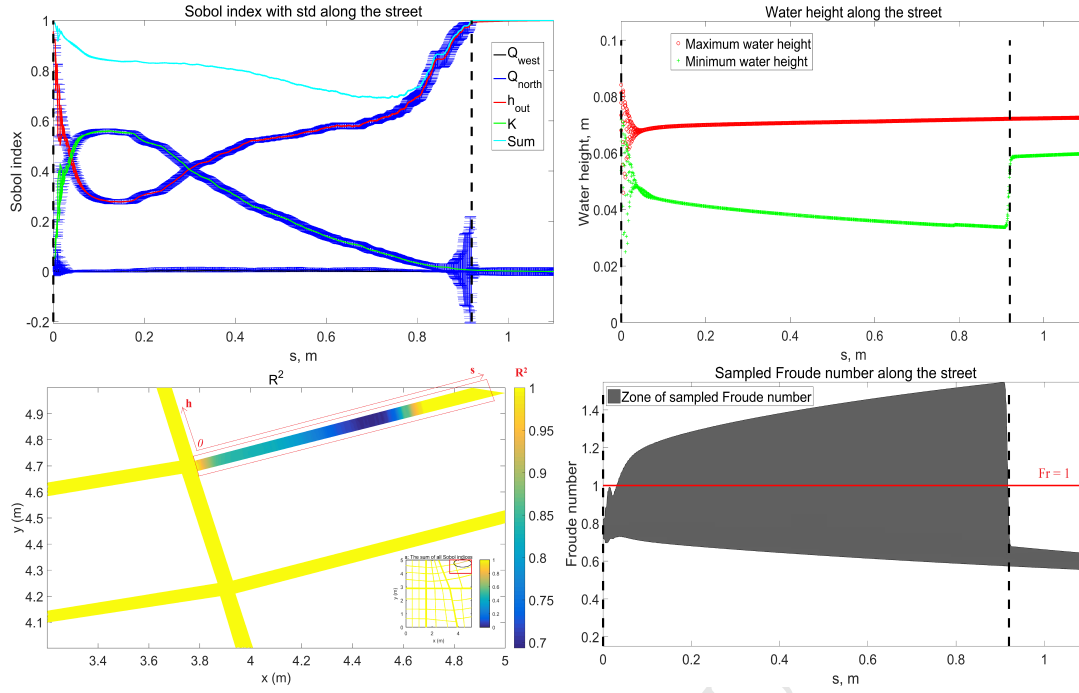


Figure 9: Sobol index profiles along the downstream part of street 1 (Top left);  $R^2$  map of the metamodel used to estimate  $S_i$ 's (Bottom left); variation range of water surface (Top right) and Froude number profiles (Bottom right) obtained with 2D SW model on the parameter set sample, vertical dashed lines indicates the zone where supercritical flows and hydraulic jumps appear on the sample.

proof of 2D SW ability in reproducing such flows since it is very close to the “real experimental” one - recall  $80 - 100 m^{1/3} \cdot s^{-1}$  is expected for plexiglass.

#### 4.2. Metamodel error on $S_i$ estimation with hydraulic shocks

As previously shown in section 3.2.2, the sum of the first order Sobol indices is significantly below 1 in the supercritical region (illustrated by the circles on figure 7). Figure 9 presents the  $S_i$  profiles along the downstream part of the street 1; figure 9 - bottom right shows the range of Froude numbers obtained on the parameter sample, which defines the “shock zone” where supercritical flows ( $Fr > 1$ ) and hydraulic jumps appear for some parameter sets. Figure 9 - top right presents all the sampled water surface profile; it highlights that the range of variation of the water height is almost 3 times larger in the shock zone compared to outside.

Downstream of the shock zone ( $x > 0.9$ ), the variance of the water height is totally explained by  $h_{out}$  (cf. figure 9 - top left); for  $x$  between 0.15 and 0.9, the sensitivity to  $h_{out}$  decreases from downstream to upstream. It can be correlated with the fact that downstream water height represents a hydraulic control only if the flow is subcritical while the most upstream point is characterized by the highest number of supercritical flows over the  $N_s$  flows simulated. The spatial variation of water height sensitivity to the roughness coefficient  $K$  is barely the negative of the sensitivity pattern to  $h_{out}$ . As presented in section 3.2.2, the sensitivity of the water height to the upstream discharge (both  $Q_{north}$  and  $Q_{west}$ ) is almost null along the whole street for the tested ranges.

However, one cannot ignore that a sum of the first order  $S_i$  lower than one claims for interaction effect between the tested parameters or for metamodel error on Sobol index (e.g. [26]). The quality of the  $S_i$  estimation with the metamodel is assessed by the correlation coefficient  $R^2$  (cf. figure 9). It appears that outside of the shock zone, the  $R^2$  is almost equal to 1 and decreases to 0.7 in the shock zone for which the water height vary of almost 50%, with respect to 10% outside, around the nominal one (figure 9). Moreover, note that metamodel standard deviation is quite narrow as shown for each  $S_i$  profile on figure 9 that remain hydraulically coherent.



#### 4.3. Sensitivity of outlet discharge

In the context of urban flood forecasting, spatial distributions of water height are of great interest as well as discharge repartition, at the downstream end of the 14 streets here. The Sobol indices of outlet discharges to 4 main flow controls ( $Q_{north}^{cal} \pm 5\%$ ,  $Q_{west}^{cal} \pm 5\%$ ;  $h_{out}^{cal} \pm 10\%$ ,  $K^{cal} \pm 50\%$ ) in figure 10 for different inflow discharge partitions (50-50% and 80-20%); Sobol indices are also calculated for subdistricts as detailed hereafter.

Figure 10, top left illustrates the Sobol indices for 14 outlets in south and east face with equal repartition of inflow discharges. For all streets, the sum of all Sobol indices is close to 1, which means no interaction effect exist between the tested parameters controlling the flow distribution at outlets. The outlet discharges in street 1, 5, 6, 7 and G are nearly totally controlled by downstream water height. We retrieve a total dependence between outlet water height and discharge, in other words a rating curve relationship for those streets. The outlets of street 5, 6, 7 and G are located at the south-east corner of the device, which is far from the inlet at west and north face, and separated by three big streets C, F and 4. Therefore, the influence of upstream discharge repartition on west and north faces can't propagate and is filtered out by those larger streets. This is confirmed by the same sensitivities to  $h_{out}$  for those streets on the 80-20% flow repartition (cf. figure 10, bottom). Moreover, concerning street 1 a supercritical flow zone occurs (cf. figures 7 and 9) hence the flow in street 1 is totally controlled by upstream conditions. Therefore the output discharge of street 1 is not controlled by its downstream water height but by those of other streets. It may be explained by the fact that, applying a stronger downstream control on all streets (i.e. increasing  $h_{out}$ ) reduces the discharge flowing out streets 2 to G thus increases relatively the discharge of street 1.

The outlets of street 2 and 3 (resp. street A, B, D and E) are located close to the inlet on north face (resp. west face), which may be the reason for higher sensitivities to  $Q_{north}$  (resp.  $Q_{west}$ ) for those streets (cf. figure 10a). The influence of  $Q_{north}$  (resp.  $Q_{west}$ ) on outlet discharge decreases from street 2 to 3 (resp. street A to E) as their distance to north-face inlet (resp. west-face inlet) increases, whereas the influence of west-face discharge (resp. north-face discharge) increases. Interestingly for streets A to E, the sensitivity of the outlet discharge to  $Q_{west}$  is divided by more than 2 between streets A-B and D-E. This may be related to the influence of the main street C between those two groups of streets.

$h_{out}$  explains around 30% of the outlet discharges of streets A-B and 60% for streets D-E. The first being located closer from the inlet hence more sensitive to inflow discharge than global outlet water height. Moreover flow is conveyed/crossing wide streets before reaching streets D-E. For big streets C, F and 4, the influence of west-face discharge and north-face discharge is equal which makes sense given their central locations within the district geometry. Interestingly, outlet discharge are barely not sensitive to a uniform roughness for those steady configurations. However, about 20% of the outlet discharge variance of street F is explained by roughness, which may be linked to its particular orientation north-west to south-east.

As observed by [14], the 14 outlet discharges can be divided into several sub-districts using big streets, which are sub-district composed of street 1 (for supercritical flow), sub-district 23, sub-district 567, sub-district AB, sub-district DE, sub-district G and sub-district 4CF composed of big streets. The Sobol indices of sub-districts are presented in figure 10 for 50-50% and 80-20% inflow repartition. When west-face discharge partition changes from 50% to 80% illustrated in figure 10, results show that the influence of west-face discharge increases at sub-district 23, sub-district AB, sub-district DE, and big street sub-district 4CF, where north-face discharge decreases respectively. The Sobol index of outlet water height and friction coefficient is not very sensitive to this change except for streets 4, A, B, C that are less (resp. more) sensitive to  $h_{out}$  (resp.  $K$ ); street F has an opposite trend. The increase of the sensitivity to  $K$  may be related to the increase of the velocity for the concerned streets.

As a conclusion of this section, wide streets act as global separators of the flow pattern into several sub-district, which can block the influence of the upstream inlet discharge and increase the influence of the downstream outlet water height.

#### 4.4. Sensitivity analysis in presence of a slope

The influence of bottom slope on the simulated free surface flows in the urban district geometry is investigated here. A constant slope in the north-south direction  $I_{NS} = 2\%$  is imposed (the increased elevation of inlets on north face is  $0.1\text{ m}$ ). The total inlet discharge is  $80\text{ m}^3/\text{h}$  with 50-50% and 80-20% discharge partitions at west and north-face. The outlet water height

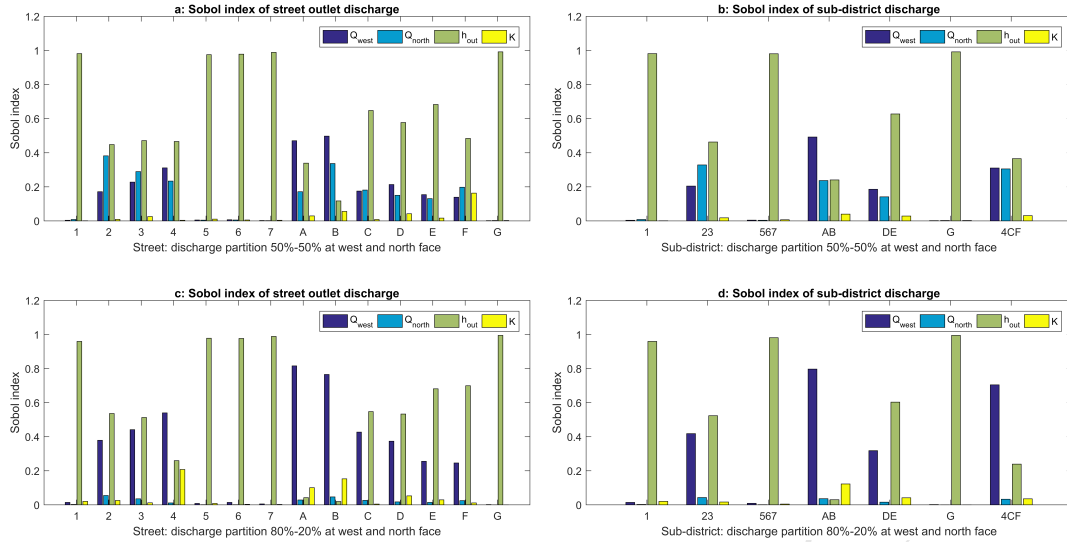


Figure 10: Sobol indices of outlet discharges obtained with the 2D SW model (for each test,  $\Sigma S_i \in [0.97; 1]$ ).

is obtained from 3D model simulations with interface tracking performed using InterFoam and validated on the measured outlet discharge in the “flat configuration” - not presented here. The four input parameters tested previously are investigated here with a bottom slope: west-face discharge  $Q_{west}^{cal} \pm 5\%$ , north-face discharge  $Q_{north}^{cal} \pm 5\%$ , uniform friction coefficient  $K^{cal} \pm 50\%$  and the downstream water height  $h_{out}$  with a range of  $\pm 10\%$  for all streets and configurations except for street 1, 2, 3 and 4 with the 80-20% inflow discharge partition because reverse flow appears at the outlet; the range is thus modified to  $[-10\%, -1\%]$ .

Figure 11 presents the results (maps of water height and Froude number) of the calibrated model with slope for both configurations and the first order Sobol index. The Froude number maps show that adding a slope in the north-south direction result in generating more supercritical flows and hydraulic jumps in streets of north-south direction than in the horizontal case. As presented in section 3.2.2, the sum of the first order Sobol index is equal to 1 for the whole subcritical flow and smaller than 1 where supercritical flows appear as shown by Froude distribution. The GSA remains consistent for the whole domain as shown in section 4.2. A comparison of Sobol index maps with and without slope (cf. figure 11 and 7) shows that the sensitivity patterns are barely the same except in the supercritical zones. In the configuration with slope, the influence of  $Q_{west}$  and  $Q_{north}$  (resp.  $h_{out}$ ) on the water height is almost multiplied (resp. divided) by 2. As in the configuration without slope, the sensitivity to roughness  $K$  becomes non negligible in the supercritical zone due to the increase of the velocity.

Histograms presented on figure 12 show the sensitivity of the water height to the tested parameters for several precise locations consisting mainly in crossroads within the streets network. They are ordered by increasing hydraulic distance from the upstream north-west corner. It clearly depicts the decrease of the sensitivity of water height to the upstream controls:  $Q_{west}$ ,  $Q_{north}$ ,  $K$ . However their influence is lower than in the previous configuration without slope (figure 8) because of the occurrence of several supercritical flow zones. The latters are characterized by a higher sensitivity to  $K$  even downstream and act as a hydraulic disconnection.

Figure 13 illustrates the influence of four input parameters on 14 outlet discharges in 50-50% inflow discharge partition with slope. Compared with the results presented in figure 10, the sum of first Sobol indices is reduced between 0.8 and 1 for all street except for streets 6 and 7 for where it reduces to almost 0.7. This can be explain by possible parameter interactions but also the occurrence of more supercritical flow zones and hydraulic jumps. Moreover streets 5 to 7 outlets are almost disconnected from upstream (due to supercritical flow in streets F and G illustrated in figure 11) and corroborates a sensitivity of outlet discharges mainly explained by  $K$  and  $h_{out}$ . The outlet discharges for the streets 5 to 7 and G are also more sensitive to the roughness coefficient  $K$  in the configuration with slope which can be related to the increase of the velocity in the southern streets. The outlet discharge for the streets 2 to 4, B, D and E are significantly less depending on  $Q_{west}$  and  $Q_{north}$  (with a similar  $S_{Q_{west}}/S_{Q_{north}}$  ratio for streets B, D and E) and conversely more depending on  $h_{out}$ . This can be related to north-south

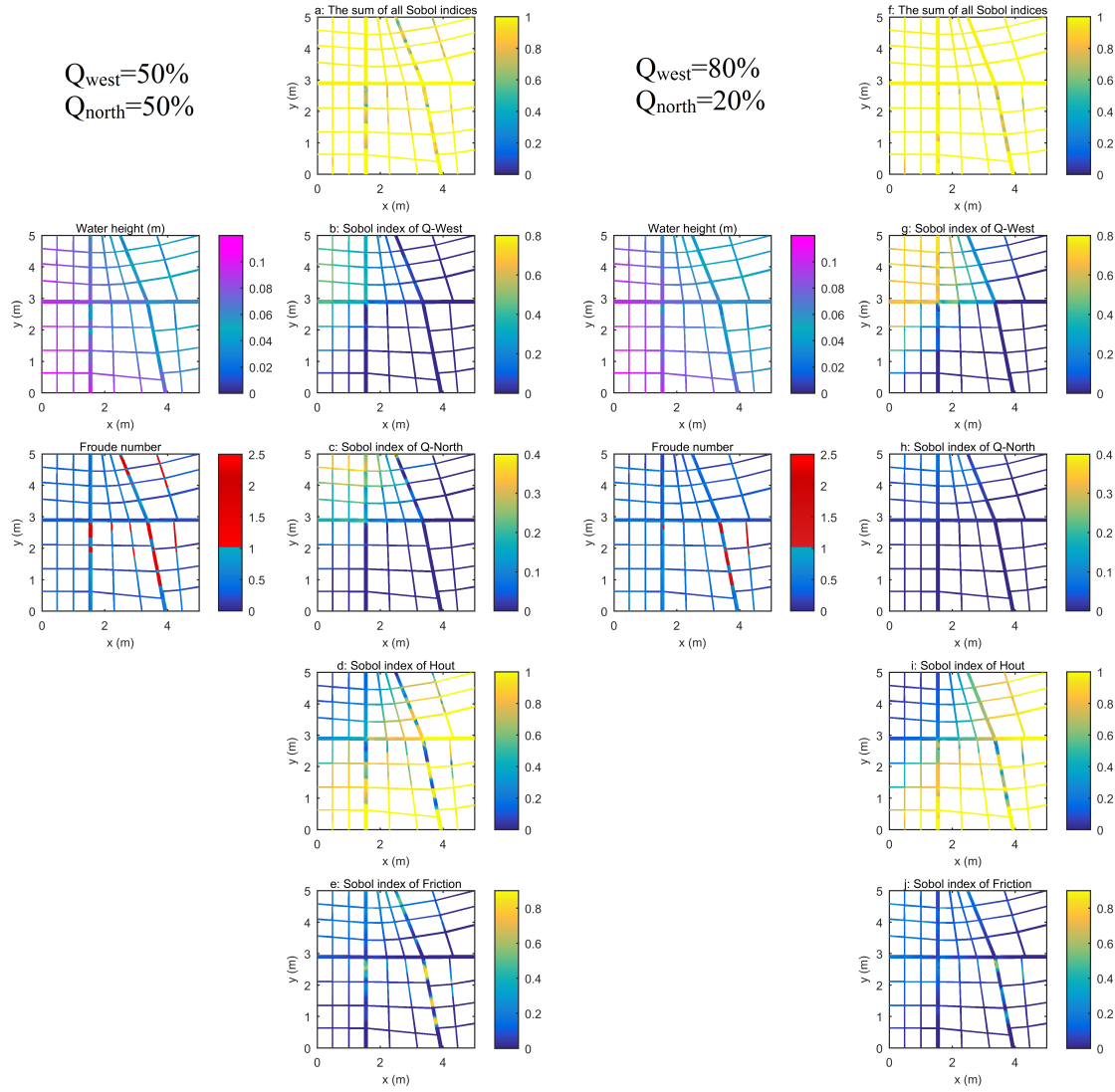


Figure 11: 2D maps of Sobol indices for  $80 \text{ m}^3/\text{h}$  with slope: Left, equal 50-50% inflow discharge partition between west and north-face; Right, 80-20% inflow discharge partition between west and north-face

slope that deviates the flow in the south and south-east outlets. No significant change can be observed for street 1 and A. The slope has an opposite effect for the main streets C and F outlet sensitivity patterns: the sensitivity to  $h_{out}$  decreases (resp. increases) for street C (resp. F). Street C becomes more sensitive to  $Q_{west}$  whereas street F becomes insensitive to both  $Q_{west}$  and  $Q_{north}$ . Those trends might be explained by more supercritical flows appearing in street F than in street C, leading to a more important deconnection from upstream.

## 5. Conclusions

This study proposes a global sensitivity analysis (GSA) of 1D and 2D shallow water models applied to flood flows in an urban district. It quantifies the sensitivity of Shallow water model outputs, the simulated water height and discharge repartition in a branched network, to the model input parameters. For our case study based on the urban flood experimental rig of ICube laboratory Strasbourg different spatial patterns of parameters sensitivity have been found and model output variance explained with respect to parameter sensitivities:

- General sensitivity patterns of 1D SW equations have been obtained with parameters sampled on equal ranges. The results show that in 1D configuration, the closer from the downstream boundary condition on water height, the higher the Sobol index as predicted by hydraulic theory for subcritical flow. Interestingly, the sensitivity to friction and upstream

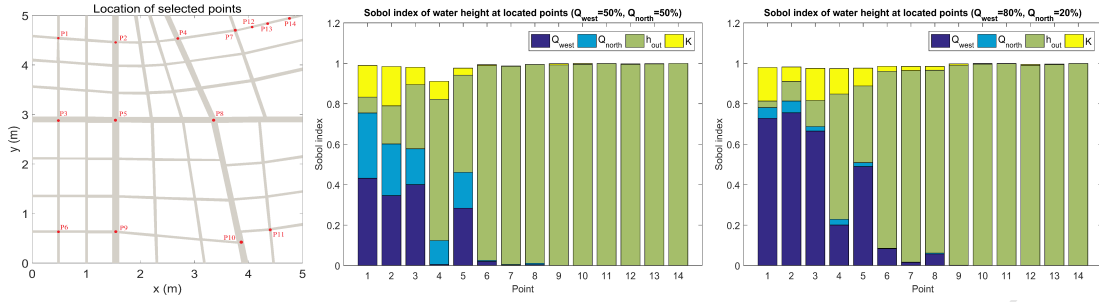


Figure 12: Decomposition of local sensitivity of water height to the tested parameters, experiment with slope. Numbering of points made in function of hydraulic distance to the upstream north-west corner.

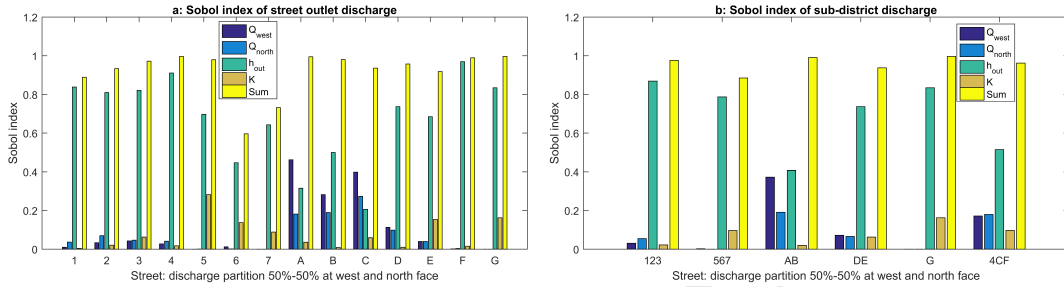


Figure 13: Sobol indices of outlet discharges obtained with the 2D SW model with slope.

discharge are very similar. At a 'far enough' upstream end of the domain, the sensitivity to the downstream water height is null and both roughness coefficient and upstream discharge explain 50% of the water height variance.

- 1D Sensitivity patterns corresponding to our experimental uncertainties are similar to previous ones with a lower influence of the upstream discharge that is less uncertain. Water height variance is mostly explained by friction and downstream water height showing opposite spatial variations. The sensitivity analysis to the lateral discharges highlight that the main (resp. smaller) streets of the experimental rig explain 30 to 45% (resp. 0 to 15%) of the water height variance with a higher sensitivity close to the crossroads at which the flow is injected. Sensitivity to distributed (street and crossroad) friction coefficient has shown that the water height variance is not proportional to the domain size on which a friction coefficient (either crossroad and street) is applied and that similar parameterization for different streets produce variables sensitivity responses. This highlights the need of identifying the strongest hydraulic controls during a calibration process.
- Maps of Sobol indices are provided for 2D SW model with two different upstream discharge partitions. The results are in agreement with the findings in 1D but in different proportions: the water height variance is explained at almost 70% by the downstream water height, to less than 10% by the friction coefficient and to less than 25% by the upstream discharge. This highlights that the friction coefficient plays a different role in the energy dissipation at 2D scale. Moreover it quantifies the filtering effect of the topography on the discharge distribution through the whole district as suggested by [14] which is confirmed by the downstream discharge sensitivity to upstream inflow that is barely null. The sensitivity of downstream discharge repartition to a uniform roughness is shown to be relatively low on the tested configurations as suggested by [4] with forward SW model runs on a Cartesian grid. Concerning the street outlet discharge, different sensitivity patterns are obtained with a variance explained at 100% by the downstream water height, or almost equally explained by the downstream water height and the upstream faces discharge; the friction coefficient being only involved in some particular streets. The key findings is that larger streets acts as global flow pattern separators into several sub-district, which can block the influence of upstream inlet discharge and increase the influence of downstream outlet water height.
- Sensitivity maps are also presented for hydraulic regime changes and flows with a positive

bottom slope triggering more supercritical flow in the district. The global sensitivity patterns remains similar but with an increased role of the friction coefficient, a water height distribution that is less downstream dependent (especially in the sub-district that is closer of the inlets), and an asymmetrical sensitivity to the upstream discharge (with an increased sensitivity to the north discharge).

This work highlights and somehow quantifies the nonlinearities of these complex free surface flow patterns and dependencies. It is based on parameter ranges estimated from experimental uncertainties, given the difficulties to access real (urban) flood data with their associated uncertainties, and could serve as a base for future works for example for propagating uncertainties from a hydrological model. Subsequent works could also investigate unsteady aspects of urban flood flows for other geometries, flood magnitude and source terms such as street/underground networks or building interactions. The sensitivity of 1D/2D coupled models could also be investigated along with other parameterizations of flow resistance. Note that the results presented involve a significant number of model runs - on the order of  $10^4$  2D model ( $4 \cdot 10^5$  cells) evaluations were needed corresponding 35 days of calculation on 256 cores. New methods for computing Sobol indices at a lower cost could also be of interest (e.g. [26]). **Studying flow paths and how they are influenced by different street blockage (including local throats due to recirculations) may be an interesting topic for further research. Also, quantifying the sensitivity trends of SW model outputs with respect to inputs should also be investigated more deeply on complex configurations with adapted techniques such as forward computations using the derivative of state variables with respect to parameters ([9]), or adjoint based methods ([30]).**

## 6. Acknowledgments

The authors warmly thank all the technicians and researchers involved in the large ICube urban flood laboratory experiment. The authors greatly acknowledge the China Scholarship Council who funded the first author. The University of Strasbourg and its high performance computing team is also greatly acknowledged for the calculation resources provided for this work.

## 7. Appendix

### 7.1. 2D shallow water equations

$$\frac{\partial \mathbf{U}}{\partial t} + \frac{\partial \mathbf{F}}{\partial x} + \frac{\partial \mathbf{G}}{\partial y} = \mathbf{S} \quad (4)$$

$$\mathbf{U} = \begin{bmatrix} h \\ q \\ r \end{bmatrix}, \mathbf{F} = \begin{bmatrix} q \\ \frac{q^2}{h} + gh^2/2 \\ \frac{qr}{h} \end{bmatrix}, \mathbf{G} = \begin{bmatrix} r \\ \frac{qr}{h} \\ \frac{r^2}{h} + gh^2/2 \end{bmatrix}, \mathbf{S} = \begin{bmatrix} 0 \\ gh(S_{0,x} - S_{f,x}) \\ gh(S_{0,y} - S_{f,y}) \end{bmatrix}$$

where the unit discharge component  $q = hu$  and  $r = hv$ ,  $S_0$  and  $S_f$  are the bottom slope and head slope.

### 7.2. 1D shallow water equations

$$\frac{\partial \mathbf{U}}{\partial t} + \frac{\partial \mathbf{F}}{\partial x} = \mathbf{S} \quad (5)$$

$$\mathbf{U} = \begin{bmatrix} h \\ q \end{bmatrix}, \mathbf{F} = \begin{bmatrix} q \\ \frac{q^2}{h} + gh^2/2 \end{bmatrix}, \mathbf{S} = \begin{bmatrix} 0 \\ gh(S_0 - S_f) \end{bmatrix}$$

where the unit discharge component  $q = hu$ ,  $S_0$  and  $S_f$  are the bottom slope and head slope.



## 7.3. Boundary conditions

Table 2: Boundary conditions for device simulation.

Street	Inlet discharge	Outlet water height	Street	Inlet discharge	Outlet water height
1	1.37 l/s	6.5 cm	A	1.06 l/s	8.3 cm
2	1.40 l/s	7.8 cm	B	1.06 l/s	8.0 cm
3	1.32 l/s	7.8 cm	C	2.67 l/s	8.3 cm
4	3.01 l/s	7.8 cm	D	1.27 l/s	7.3 cm
5	1.32 l/s	6.4 cm	E	1.27 l/s	7.1 cm
6	1.35 l/s	6.5 cm	F	2.46 l/s	7.1 cm
7	1.35 l/s	6.5 cm	G	1.31 l/s	6.4 cm

## References

- [1] Morgan Abily, Nathalie Bertrand, Olivier Delestre, Philippe Gourbesville, and Claire-Marie Duluc. Spatial global sensitivity analysis of high resolution classified topographic data use in 2d urban flood modelling. *Environmental Modelling & Software*, 77:183–195, 2016.
- [2] IPCC Adopted. Climate change 2014 synthesis report. 2014.
- [3] Quentin Araud. *Simulations des écoulements en milieu urbain lors d’un évènement pluvieux extrême*. PhD thesis, Université de Strasbourg, 2012.
- [4] Anaïs Arrault, Pascal Finaud-Guyot, Pierre Archambeau, Martin Bruwier, Sébastien Erpicum, Michel Piroton, and Benjamin Dewals. Hydrodynamics of long-duration urban floods: experiments and numerical modelling. *Natural Hazards and Earth System Sciences*, 16(6):1413–1429, 2016.
- [5] Keith Beven and Andrew Binley. The future of distributed models: model calibration and uncertainty prediction. *Hydrological processes*, 6(3):279–298, 1992.
- [6] P. Brisset, P. Garambois, J. Monnier, and H. Roux. Identifiability and assimilation of sparse altimetry data in 1d saint-venant river models. *Advances in Water Resources revised*, 2018.
- [7] Ludovic Cassan, Gilles Belaud, Jean Pierre Baume, Cyril Dejean, and Frederic Moulin. Velocity profiles in a real vegetated channel. *Environmental Fluid Mechanics*, 15(6):1263–1279, 2015.
- [8] Ludovic Cassan, Hélène Roux, and Pierre-André Garambois. A semi-analytical model for the hydraulic resistance due to macro-roughnesses of varying shapes and densities. *Water*, 9(9):637, 2017.
- [9] Carole Delenne, Pascal Finaud-Guyot, Vincent Guinot, and Bernard Cappelaere. Sensitivity of the 1d shallow water equations with source terms: Solution method for discontinuous flows. *International Journal for Numerical Methods in Fluids*, 67(8):981–1003, 2011.
- [10] Guy Delrieu, John Nicol, Eddy Yates, Pierre-Emmanuel Kirstetter, Jean-Dominique Creutin, Sandrine Anquetin, Charles Obled, Georges-Marie Saulnier, Véronique Ducrocq, Eric Gaume, et al. The catastrophic flash-flood event of 8–9 september 2002 in the gard region, france: a first case study for the cévennes–vivaraïs mediterranean hydrometeorological observatory. *Journal of Hydrometeorology*, 6(1):34–52, 2005.
- [11] F Dottori, G Di Baldassarre, and E Todini. Detailed data is welcome, but with a pinch of salt: Accuracy, precision, and uncertainty in flood inundation modeling. *Water Resources Research*, 49(9):6079–6085, 2013.
- [12] Audrey Douinot, Hélène Roux, and Denis Dartus. Modelling errors calculation adapted to rainfall–runoff model user expectations and discharge data uncertainties. *Environmental Modelling & Software*, 90:157–166, 2017.

- [13] Charlotte M Emery, Sylvain Biancamaria, Aaron Boone, Pierre-André Garambois, Sophie Ricci, Mélanie C Rochoux, and Bertrand Decharme. Temporal variance-based sensitivity analysis of the river-routing component of the large-scale hydrological model isba-trip: Application on the amazon basin. *Journal of Hydrometeorology*, 17(12):3007–3027, 2016.
- [14] P Finaud-Guyot, P-A Garambois, Q Araud, F Lawniczak, P François, J Vazquez, and R Mosé. Experimental insight for flood flow repartition in urban areas. *Urban Water Journal*, pages 1–9, 2018.
- [15] Pierre-André Garambois, Hélène Roux, Kévin Larnier, William Castaings, and Denis Dartus. Characterization of process-oriented hydrologic model behavior with temporal sensitivity analysis for flash floods in mediterranean catchments. *Hydrology and Earth System Sciences*, 17:2305–2322, 2013.
- [16] Pierre-André Garambois, Hélène Roux, Kévin Larnier, David Labat, and Denis Dartus. Parameter regionalization for a process-oriented distributed model dedicated to flash floods. *Journal of Hydrology*, 525:383–399, 2015.
- [17] Rodger Grayson and Günter Blöschl. *Spatial patterns in catchment hydrology: observations and modelling*. CUP Archive, 2001.
- [18] Vincent Guinot. Multiple porosity shallow water models for macroscopic modelling of urban floods. *Advances in Water Resources*, 37:40–72, 2012.
- [19] Vincent Guinot. *Wave propagation in fluids: models and numerical techniques*. John Wiley & Sons, 2012.
- [20] Vincent Guinot and Bernard Cappelaere. Sensitivity analysis of 2d steady-state shallow water flow. application to free surface flow model calibration. *Advances in Water Resources*, 32(4):540–560, 2009.
- [21] Vincent Guinot and Bernard Cappelaere. Sensitivity equations for the one-dimensional shallow water equations: Practical application to model calibration. *Journal of Hydrologic Engineering*, 14(8):858–861, 2009.
- [22] Vincent Guinot and Sandra Soares-Frazão. Flux and source term discretization in two-dimensional shallow water models with porosity on unstructured grids. *International Journal for Numerical Methods in Fluids*, 50(3):309–345, 2006.
- [23] Jean-Michel Hervouet. Telemac modelling system: an overview. *Hydrological Processes*, 14(13):2209–2210, 2000.
- [24] Jean-Michel Hervouet. *Hydrodynamics of free surface flows: modelling with the finite element method*. John Wiley & Sons, 2007.
- [25] George M Hornberger and Robert C Spear. Approach to the preliminary analysis of environmental systems. *J. Environ. Mgmt.*, 12(1):7–18, 1981.
- [26] Alexandre Janon. *Analyse de sensibilité et réduction de dimension. Application à l’océanographie*. PhD thesis, Université de Grenoble, 2012.
- [27] E Mignot, A Paquier, and S Haider. Modeling floods in a dense urban area using 2d shallow water equations. *Journal of Hydrology*, 327(1):186–199, 2006.
- [28] H de Moel, J van Alphen, and JCJH Aerts. Flood maps in europe—methods, availability and use. *Natural Hazards and Earth System Sciences*, 9(2):289–301, 2009.
- [29] Adrien Momplot, Gislain Lipeme Kouyi, Emmanuel Mignot, Nicolas Rivière, and Jean-Luc Bertrand-Krajewski. Typology of the flow structures in dividing open channel flows. *Journal of Hydraulic Research*, 55(1):63–71, 2017.
- [30] Jérôme Monnier, Frédéric Couderc, D Dartus, K Larnier, R Madec, and J-P Vila. Inverse algorithms for 2d shallow water equations in presence of wet dry fronts: Application to flood plain dynamics. *Advances in Water Resources*, 97:11–24, 2016.

- [31] Jeffrey Neal, Ignacio Villanueva, Nigel Wright, Thomas Willis, Timothy Fewtrell, and Paul Bates. How much physical complexity is needed to model flood inundation? *Hydrological Processes*, 26(15):2264–2282, 2012.
- [32] Adrien Paris, Rodrigo Dias de Paiva, Joecila Santos da Silva, Daniel Medeiros Moreira, Stephane Calmant, Pierre-André Garambois, Walter Collischonn, Marie-Paule Bonnet, and Frederique Seyler. Stage-discharge rating curves based on satellite altimetry and modeled discharge in the amazon basin. *Water Resources Research*, 2016.
- [33] Francesca Pianosi, Keith Beven, Jim Freer, Jim W Hall, Jonathan Rougier, David B Stephenson, and Thorsten Wagener. Sensitivity analysis of environmental models: A systematic review with practical workflow. *Environmental Modelling & Software*, 79:214–232, 2016.
- [34] Raji Pushpalatha, Charles Perrin, Nicolas Le Moine, Thibault Mathevet, and Vazken Andréassian. A downward structural sensitivity analysis of hydrological models to improve low-flow simulation. *Journal of Hydrology*, 411(1):66–76, 2011.
- [35] Marco Ratto, Andrea Pagano, and Peter Young. State dependent parameter metamodelling and sensitivity analysis. *Computer Physics Communications*, 177(11):863–876, 2007.
- [36] Hélène Roux and Denis Dartus. Sensitivity analysis and predictive uncertainty using inundation observations for parameter estimation in open-channel inverse problem. *Journal of Hydraulic Engineering*, 134(5):541–549, 2008.
- [37] Andrea Saltelli, Paola Annoni, Ivano Azzini, Francesca Campolongo, Marco Ratto, and Stefano Tarantola. Variance based sensitivity analysis of model output. design and estimator for the total sensitivity index. *Computer Physics Communications*, 181(2):259–270, 2010.
- [38] Andrea Saltelli, Marco Ratto, Terry Andres, Francesca Campolongo, Jessica Cariboni, Debora Gatelli, Michaela Saisana, and Stefano Tarantola. *Global sensitivity analysis: the primer*. John Wiley & Sons, 2008.
- [39] Andrea Saltelli, Stefano Tarantola, Francesca Campolongo, and Marco Ratto. *Sensitivity analysis in practice: a guide to assessing scientific models*. John Wiley & Sons, 2004.
- [40] IM SOBOL. Sensitivity analysis for nonlinear mathematical models. *Mathematical Modeling & Computational Experiment*, 1:407–414, 1993.
- [41] James Thomas Steven Savage, Francesca Pianosi, Paul Bates, Jim Freer, and Thorsten Wagener. Quantifying the importance of spatial resolution and other factors through global sensitivity analysis of a flood inundation model. *Water Resources Research*, 52(11):9146–9163, 2016.
- [42] Tien Dung Tran, Jacques Chorda, Pascale Laurens, and Ludovic Cassan. Modelling nature-like fishway flow around unsubmerged obstacles using a 2d shallow water model. *Environmental Fluid Mechanics*, 16(2):413–428, 2016.
- [43] Benoît Vié, Olivier Nuissier, and Véronique Ducrocq. Cloud-resolving ensemble simulations of mediterranean heavy precipitating events: uncertainty on initial conditions and lateral boundary conditions. *Monthly Weather Review*, 139(2):403–423, 2011.
- [44] SE Werners, F Ludwig, et al. Water resources in europe in the context of vulnerability. Technical report, European Environment Institute, 2012.

**Highlights:**

- GSA framework for branched urban flood flows modeling.
- Sobol spatial sensitivities of 1D and 2D shallow water models.
- Identification of hydraulic controls for various uncertainty combinations.
- Filtering effect of branched network topography quantified.